ADVANCED MATERIALS

Supporting Information

for *Adv. Mater.,* DOI: 10.1002/adma.202210794

Control of Host-Matrix Morphology Enables Efficient Deep-Blue Organic Light-Emitting Devices

*Haonan Zhao, Jongchan Kim, Kan Ding, Mina Jung, Yongxi Li, Harald Ade, Jun Yeob Lee, and Stephen R. Forrest**

Supplementary Information

Control of Host-Matrix Morphology Enables Efficient Deep-Blue Organic Light-Emitting Devices

Haonan Zhao[1+], Jongchan Kim[2+#], Kan Ding[4], Mina Jung[5], Yongxi Li[1], Harald Ade[4], Jun Yeob Lee[5], Stephen R. Forrest[1,3*]

[1] Department of Physics, University of Michigan, Ann Arbor, MI, USA
[2] Department of Electrical and Computer Engineering, University of Michigan, Ann Arbor, MI, USA
[3] Department of Materials Science and Engineering, University of Michigan, Ann Arbor, MI, USA
[4] Department of Physics, North Carolina State University, Raleigh, NC, USA
[5] School of Chemical Engineering, Sungkyunkwan University, Suwon, Gyeonggi, Korea

 # Current address: Department of Computer Integrated Display Engineering, Yonsei University, Seoul, Republic of Korea

*email: stevefor@umich.edu

S1. Cyclic voltammetry of SiTrzCz2

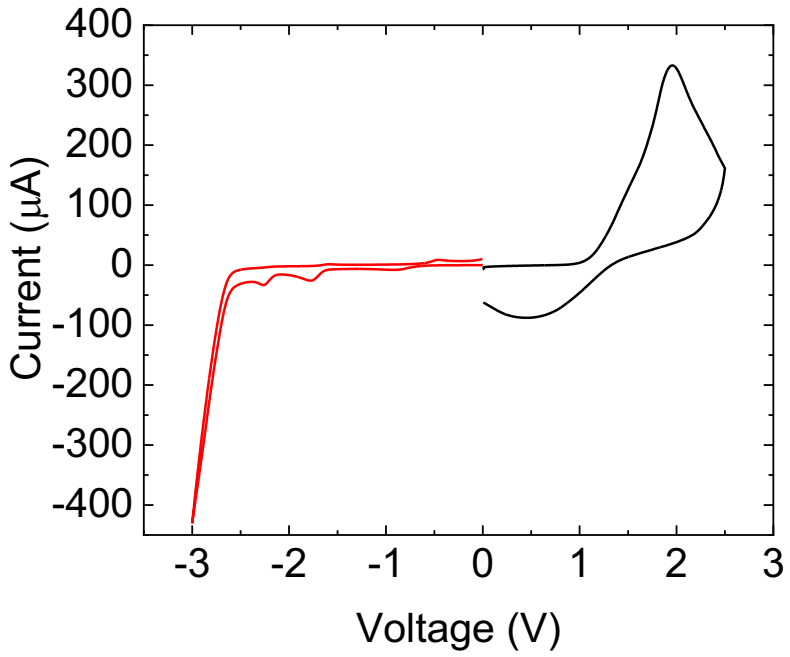

Figure S1. Cyclic voltammetry. The voltammogram of SiTrzCz2 vs. a ferrocene reference. The working reference, and the counter electrodes were C, Ag, and Pt, respectively. The voltage was applied between -3V to 2.5V with the interval of 0.05V (Ivium Stat).

S2. Differential scanning calorimetry measurements of mixed host films

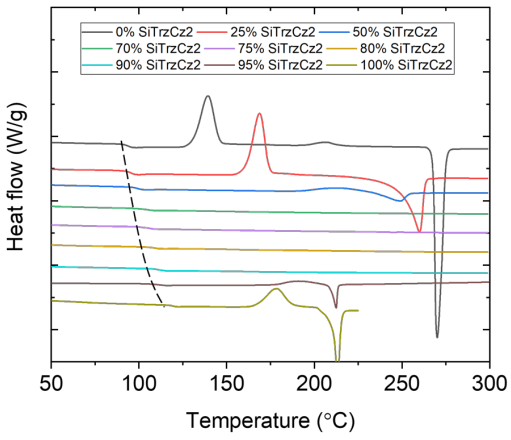

Figure S2. Differential scanning calorimetry. Differential scanning calorimetry (DSC) data obtained using a Seiko Exstar 6000 (DSC6100) from 40 to 300 °C at a heating rate of 10 °C/min under a nitrogen atmosphere. All samples were 3 - 4 mg and sealed in a hermetic Al pan. The first

thermal scan melted the blends at 300 °C for 5 min followed by rapid cooling to form a well-mixed, amorphous state. The T_g and T_m are extracted from the onset of the dips of the second and the following scans. The T_c are extracted from the positions of the recrystallization peaks.

The glass transition temperature T_g increases with SiTrzCz2 fraction, reaching a peak for a neat SiTrzCz2 film. Note that the crystallization temperature T_c and the melting point T_m vanish in the region between 55%-90% for SiTrzCz2, proving a fully suppressed crystallization.

S3. GIWAXS pattern of Annealed films

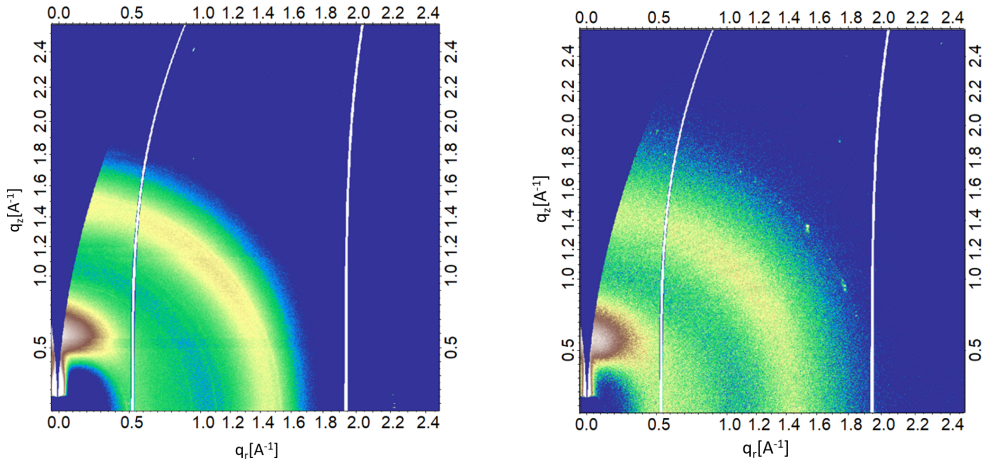

Table S3-1: GWACS Data

		Location ($Å^{-1}$)	Stacking Distance (Å)	FWHM ($Å^{-1}$) [(a)]	Orientation
Neat mCBP	π-π Stack	1.49	4.21	0.33 ± 0.01	Isotropic
	Lamellar	0.623	10.1	0.23 ± 0.01	Out-of-plane
Mixed	π-π Stack	1.50	4.19	0.45 ± 0.01	Isotropic
	Lamellar	0.60	10.50	0.24 ± 0.01	Out-of-plane

Figure S3-1 and Table S3-1. Grazing-Incidence Wide-Angle X-ray Scattering (GIWAXS) patterns for films annealed at 40°C. Left: Neat mCBP host doped with 20% $Ir(cb)_3$. Right: 1:1 mixed host film.

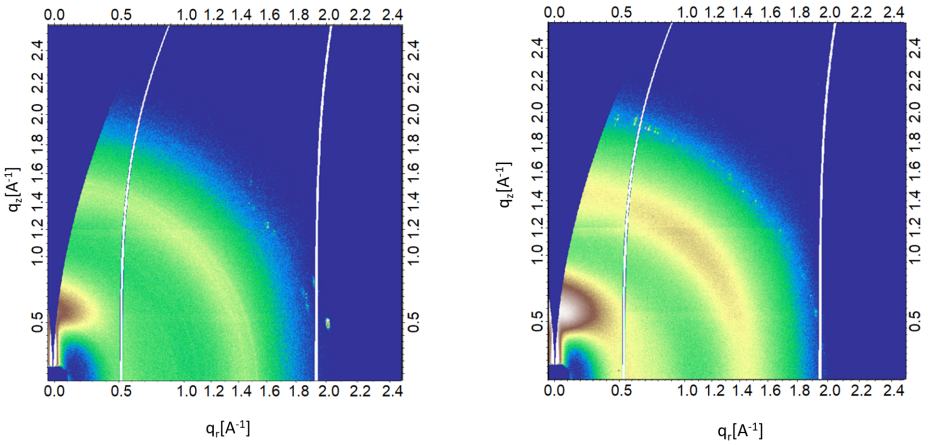

Table S3-2: GWACS Data

		Location ($Å^{-1}$)	Stacking Distance (Å)	FWHM ($Å^{-1}$) [a]	Orientation
Neat mCBP	π-π Stack	1.47	4.27	0.24 ± 0.01	Isotropic
	Lamellar	0.656	9.57	0.24 ± 0.01	Out-of-plane
Mixed	π-π Stack	1.48	4.24	0.40 ± 0.02	Isotropic
	Lamellar	0.60	10.50	0.26 ± 0.01	Out-of-plane

Figure S3-2 and Table S3-2. Films annealed at 60°C. Left: Neat mCBP host doped with 20% $Ir(cb)_3$. Right: 1:1 mixed host film.

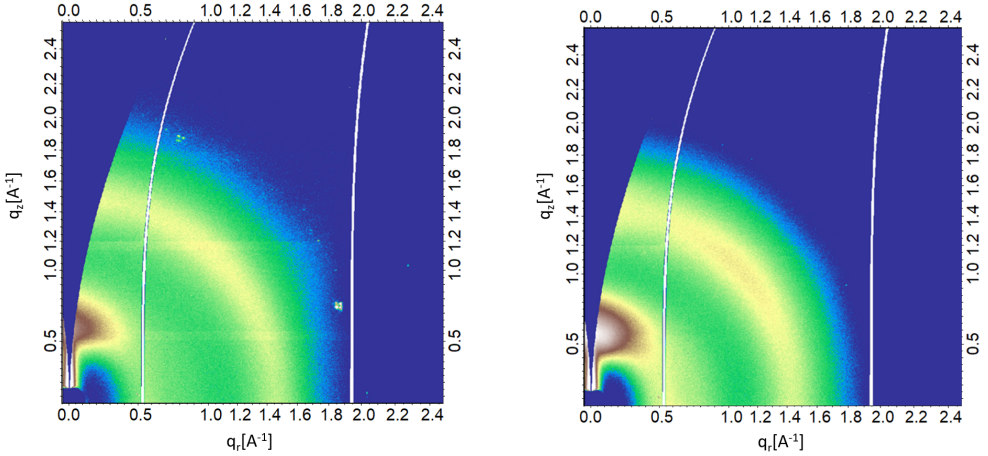

Table S3-3: GWACS Data

		Location ($Å^{-1}$)	Stacking Distance (Å)	FWHM ($Å^{-1}$) [a]	Orientation
Neat mCBP	π-π Stack	1.50	4.19	0.33 ± 0.01	Isotropic
	Lamellar	0.622	10.10	0.23 ± 0.01	Out-of-plane
Mixed	π-π Stack	1.49	4.21	0.45 ± 0.02	Isotropic
	Lamellar	0.606	10.40	0.22 ± 0.01	Out-of-plane

Figure S3-3 and Table S3-3. Films annealed at 80°C. Left: Neat mCBP host doped with 20% Ir(cb)$_3$. Right: 1:1 mixed host film.

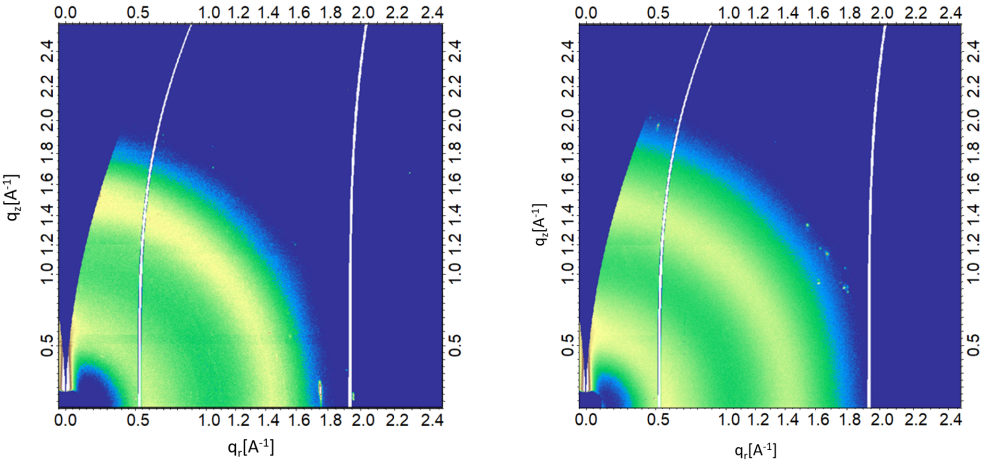

Table S3-4: GWACS Data

		Location (Å^{-1})	Stacking Distance (Å)	FWHM (Å^{-1}) [(a)]	Orientation
Neat mCBP	π-π Stack	1.51	4.16	0.31 ± 0.01	Isotropic
	Lamellar	0.602	10.40	0.33 ± 0.01	Isotropic
Mixed	π-π Stack	1.49	4.21	0.45 ± 0.02	Isotropic
	Lamellar	0.664	9.46	0.39 ± 0.02	Isotropic

Figure S3-4 and Table S3-4. Films annealed at 100°C. Left: Neat mCBP host doped with 20% Ir(cb)$_3$. Right: 1:1 mixed host film.

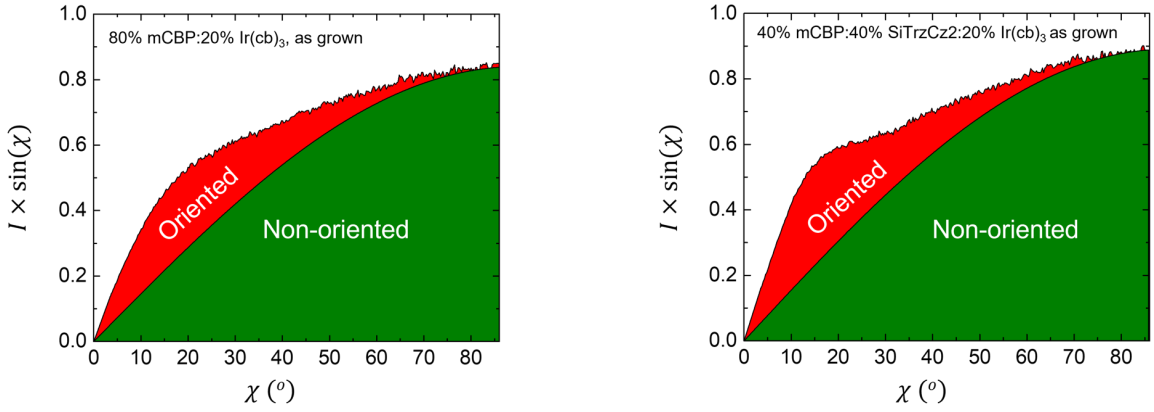

Figure S3-5 Molecular orientation distribution extracted from the GIWAXS data. Left: As grown neat mCBP host doped with 20% Ir(cb)$_3$. Right: As grown 1:1 mixed host doped with 20% Ir(cb)$_3$. Both figures show similar molecule orientation distributions.

S4. Time Resolved Photoluminescence vs. doping concentration

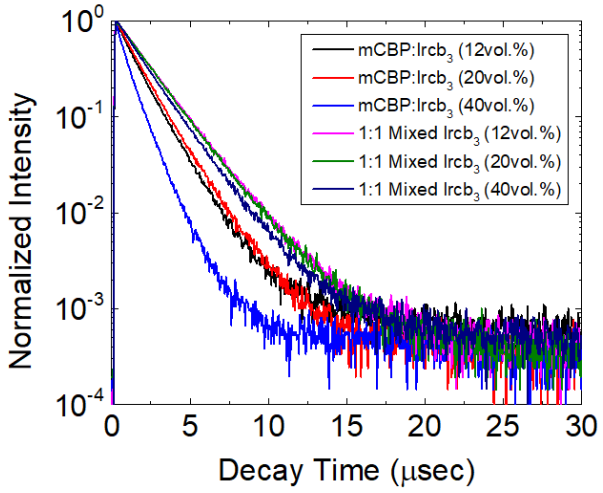

Table S4: PL Transient Data

Sample	12 Vol.%	20 Vol.%	40 Vol.%
Single mCBP	1.32 ± 0.05	1.46 ± 0.03	0.82 ± 0.04
1:1 Mixed	2.01 ± 0.04	2.01 ± 0.05	1.76 ± 0.03

†Lifetime in μs scale

Figure S4 and Table S4. Time resolved photoluminescence of mCBP single host and 1:1 mCBP:SiTrzCz2 mixed host with varied Ir(cb)$_3$ doping concentration.

S5. Photoluminescence quantum yield modeling

The PLQY is defined as[1]:

$$\Phi_{PLQY} = \frac{k_{rT}}{k_{rT} + k_{nrT}}$$

where k_{rT} is the exciton radiative decay rate, and k_{nrT} is the nonradiative decay rate. From the measured transient photoluminescent lifetime and the exciton decay rate, $k_{rT} + k_{nrT}$, is obtained. Then the radiative decay rate of the triplet excitons (k_{rT}) is obtained by dividing the PLQY with the time constant of the transient photoluminescence:

Table S5: PLQY Yields vs Doping

Sample		12 Vol.%	20 Vol.%	40 Vol.%
Single mCBP	Rad	0.39 ± 0.12	0.38 ± 0.11	0.40 ± 0.16
	Non-rad	0.36 ± 0.12	0.31 ± 0.11	0.82 ± 0.17
1:1 Mixed	Rad	0.40 ± 0.10	0.42 ± 0.10	0.36 ± 0.11
	Non-rad	0.09 ± 0.10	0.07 ± 0.10	0.20 ± 0.11

†Unit omitted for all data points (per microsecond)

S6. Nonradiative recombination, triplet-polaron annihilation and triplet-triplet annihilation modeling for OLEDs

For the transient study, $n(t)$, $J\sim0$ and TPA is not present since the transients are measured after the voltage turn-off. We discuss two scenarios as below:

$$\begin{cases} \dfrac{dT(t)}{dt} = -(k_{rT} + k_{nrT})T(t) - \dfrac{1}{2}k_{TTA}T(t)^2, & k_{nrT} = constant, \quad (guest - guest\ TTA) \\ \dfrac{dT(t)}{dt} = -(k_{rT} + k_{nrT})T(t), & k_{nrT} = k_{QT}Q_0(J)e^{-\frac{t}{\tau_Q}}, \quad (our\ model) \end{cases}$$

The relative EQE is: $\frac{\eta_{EQE}}{\eta_0} = \frac{k_{rT}+k_{nrT,0}}{k_{rT}+k_{nrT}} = \frac{\tau}{\tau_0}$. The fitted rates in both models are shown in Fig. S6-1c-d.

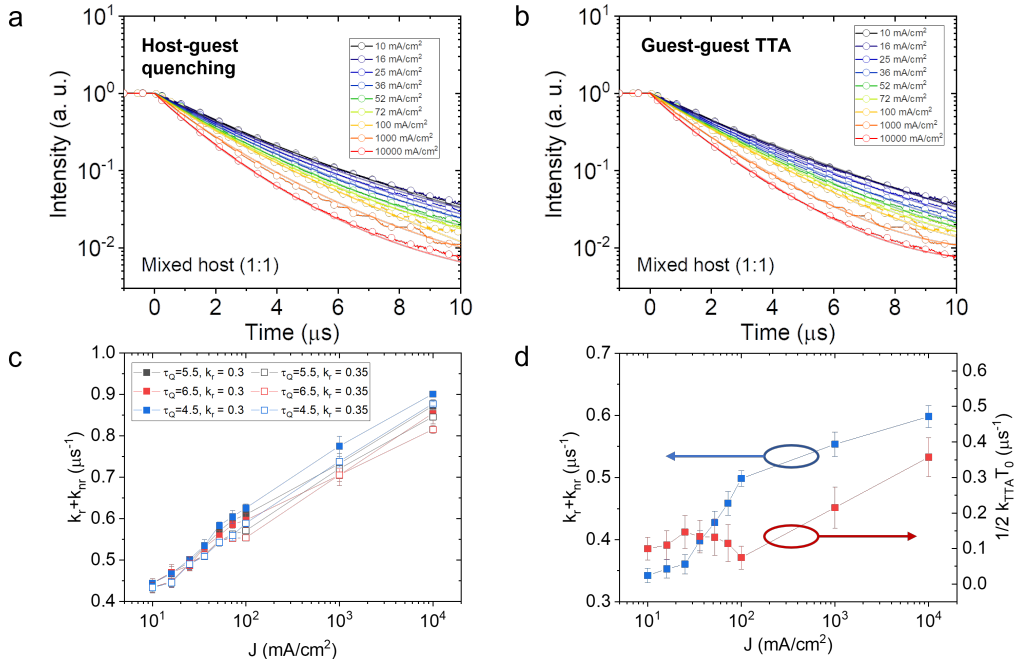

Figure S6-1. Fitting of EL transients of the 1:1 mixed host device vs. injected current density. The transients are fitted to (a) host-guest quenching model and (b) guest-guest TTA model. Extracted

decay rate contributions from each term are plotted for (c) host-guest quenching model and (d) guest-guest TTA model.

The neat mCBP device does not show a typical TPA or TTA roll-off. In steady state, considering conventional TPA with $n(t) \propto j^{\frac{1}{m+1}}$ and guest-guest TTA, and the external quantum efficiency (EQE) becomes

$$\frac{\eta_{EQE}}{\eta_0} = \frac{k_T^2 ed}{2k_{TTA}J}\left[\sqrt{\left(1+\frac{k_{TPA}n_0}{k_T}J^{\frac{1}{m+1}}\right)+4\frac{Jk_{TTA}}{k_T^2 ed}}-\left(1+\frac{k_{TPA}n_0}{k_T}J^{\frac{1}{m+1}}\right)\right],$$

where η_0 is the EQE without nonradiative recombination, TPA, or TTA, n_0 is the carrier density at unit current density, and we take $m \sim 1$ corresponding to the SCLC regime. k_{TPA} and k_{TTA} contribute to the EQE roll-off.

The mCBP host device shows the same EL lifetime with increasing current density (see Fig. 5c), showing nearly saturated quenching channels. If we fit the EQE of the mCBP single host EML using the conventional TPA and guest-guest TTA model[1–3]:

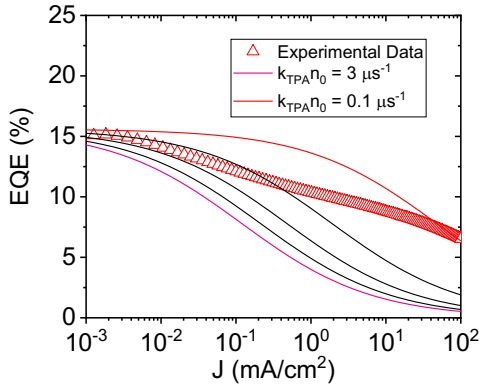

Figure S6-2. Trial TPA/TTA modeling for mCBP single host device. Assumed TPA/TTA roll-off starts from 10^{-3} mA/cm^2.

where the k_{TTA} is 10^{-14} cm^{3}s^{-1}, and the trial $k_{TPA}n_0$ ranges between 0.1 μs^{-1} to 3 μs^{-1} . The measured EQE curve does not match the typical TPA roll-off feature. This may be due to nonradiative recombination between mCBP and Ir(cb)$_3$ mentioned above as well as a shifted recombination zone. The latter is caused by the mobility mismatch between the electrons and holes within the emissive layer since the electrons are carried by the sparse dopant molecules whereas the holes are carried by the host matrix.

S7. DFT Simulation Results

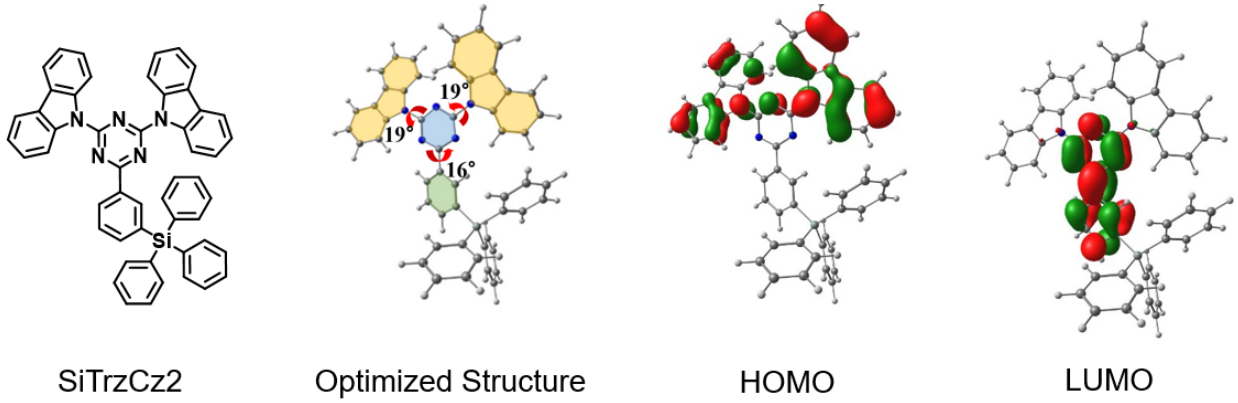

Table S7: DFT Results

Material	Oscillator Strength (*f*)	S_1 (eV)	T_1 (eV)	$\triangle E_{ST}$ (eV)	B_g (eV)	LUMO (eV)	HOMO (eV)
SiTrzCz2	0.0487	3.45	3.11	0.34	3.97	-1.78	-5.75

Figure S7 and Table S7. DFT calculations of SiTrzCz2 molecule.

S8. Optical Properties of SiTrzCz2

(a) Solution

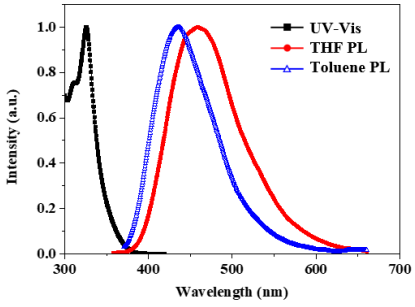

** UV-Vis was measured in THF solution*

UV (onset)	3.37 eV
PL THF (peak)	2.70 eV
PL Toluene (peak)	2.85 eV

(b) Neat film

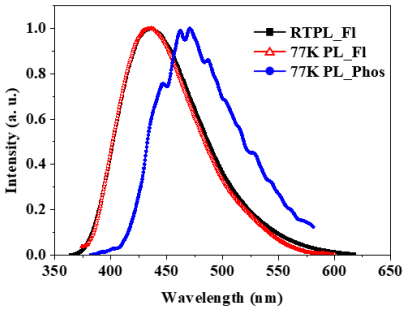

RTPL Fl (peak/onset)	2.84/3.32 eV
77K PL Fl(peak/onset)	2.84/3.30 eV
77K PL Phos(peak/onset)	2.64/3.04 eV
77K PL Phos(shoulder)	2.78 eV

(c) Solution

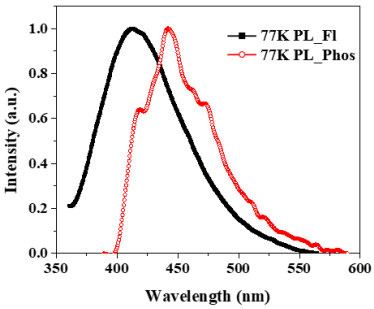

** LTPL was measured in THF solution*

77K PL Fl (peak)	3.00 eV
77K PL Phos (shoulder)	2.96 eV

Figure S8 (a) Room-temperature UV-Vis spectra and PL spectra of SiTrzCz2 in solution. (b) Room-temperature and 77K PL spectra of the SiTrzCz2 neat film. (c) 77K PL spectra of SiTrzCz2 in solution.

S9. Optical Properties of the mixed film comprising SiTrzCz2

(a) mCBP:SiTrzCz2 mixed film

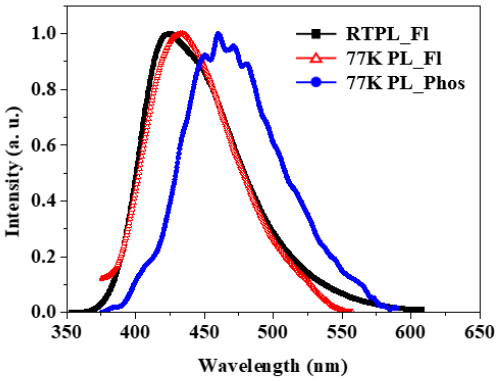

** Fabricated by evaporation process*

RTPL Fl (peak/onset)	2.91/3.30 eV
77K PL Fl(peak/onset)	2.86/3.27 eV
77K PL Phos(peak/onset)	2.70/3.20 eV
77K PL Phos(shoulder)	3.06 eV

(b) oCBP: SiTrzCz2 mixed film

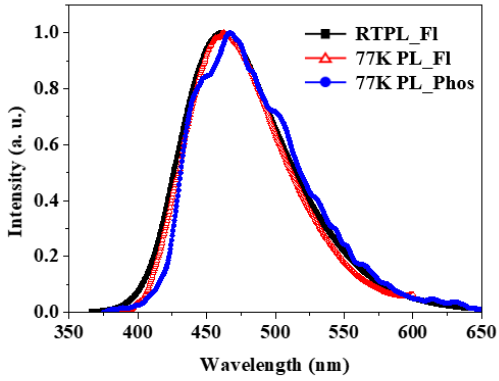

RTPL Fl (peak/onset)	2.69/3.13 eV
77K PL Fl(peak/onset)	2.69/3.09 eV
77K PL Phos(peak/onset)	2.67/3.07 eV
77K PL Phos(shoulder)	2.77 eV

Figure S9. (a) Room-temperature and 77K PL spectra of mCBP:SiTrzCz2 mixed film. (b) Room-temperature and 77K PL spectra of oCBP:SiTrzCz2 mixed film.

S10. Fourier plane imaging microscopy of the emissive layer photoluminescence vs. SiTrzCz2 concentration.

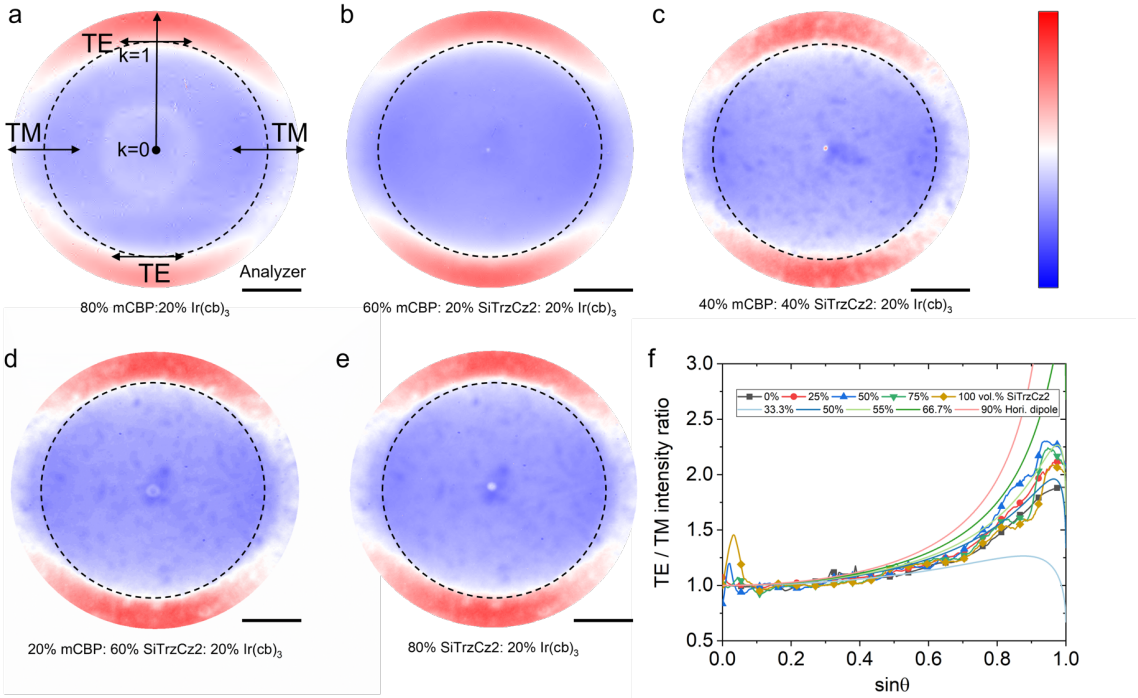

Figure S10. PL imaging in the Fourier space of mixed host emissive layers with varied SiTrzCz2 concentration.

K-space PL imaging of mixed host emissive layers with various SiTrzCz2 concentrations are shown in Fig. S10-1. The dipole orientation is determined by the ratio of intensity of TE / TM modes. A vertical dipole only has TM modes while a horizontal dipole has both TE and TM modes. All five samples show similar dipole orientations, lying between 50% - 55%, compared to the Dyadic Green's function simulation as shown by the solid lines in Fig. S10f. An isotropic orientation means 2/3 dipoles are horizontal on average.

S11. Charge balance factor analysis

The EQE can be described by the following equation[12]:

$$EQE = \eta_{int}\eta_{out} = \gamma\chi_{ST}\eta_{PL}\eta_{out}$$

γ is the charge balance factor, χ_{ST} is the emissive to total exciton formation ratio, η_{PL} is the PLQY and η_{out} is the outcoupling efficiency. In heavy-metal phosphor OLED, the $\chi_{ST} = 1$[12]. The

product of the charge balance factor and outcoupling efficiency is then EQE/PLQY. The product of peak charge balance factor and the outcoupling efficiency for varied mixed host matrix is plotted in Fig. S11, showing a deviation no greater than 4%. Thus, the EQE_{max} enhancement is mainly attributed to PLQY change.

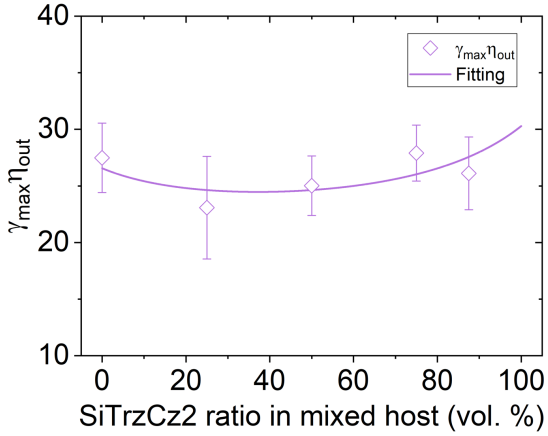

Figure S11. The product of the peak charge balance factor and the outcoupling efficiency.

S12. Mixed host and mCBP single host device operational lifetime measurements

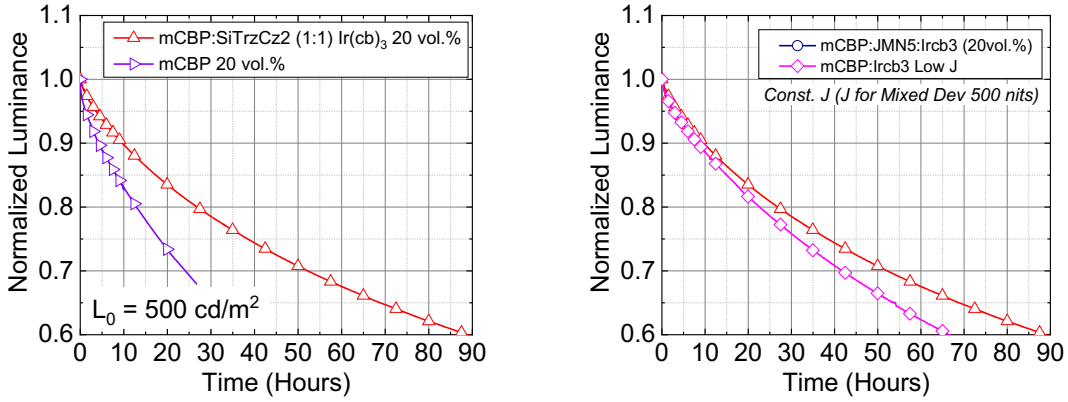

Figure S12. Luminance vs. time of PHOLEDs comprising a mCBP single host and a 1:1 mixed host. Left: Initial luminances are L_0 = 500 cd/m^2 for both devices. Right: Same current density for both devices, *J* corresponding to the initial luminance of 500cd/m^2 for the 1:1 mixed host device.

Table S13. Reported performance of deep blue OLEDs with CIEy < 0.20.

Dopant Emitter	EQE	Lifetime		L_0 (cd/m^2)	CIE(x, y)	Reference
Heavy metal phosphors						
$Ir(cb)_3$	22.5%	LT70	53 h	500	(0.14, 0.15)	This work
$Ir(cb)_3$	20.3%	LT50	8,460 h	100	(0.14, 0.19)	Ref. 3
H:Ir3 (10 wt%)	16.0%	LT70	12 h	500	(0.14, 0.17)	Ref. 4
H:Ir3 (20 wt%)	24.8%	LT70	20 h	500	(0.14, 0.18)	Ref. 4
PtON-TBBI	23.4%	LT70	1,113 h	1000	(0.14, 0.20)	Ref. 5
oCBP:mSiTrz	21.4%	LT50	1,900 h	100	(0.14, 0.16)	Ref.6
Sensitized Thermally Activated Delayed Fluorescence						
PPCzTrz/v-DABNA	25.2%	LT50	151	1000	(0.13, 0.20)	Ref. 6
PCzTrz/v-DABNA	23.8%	LT50	113	1000	(0.12, 0.18)	Ref. 6
HDT-1/v-DABNA	20%	LT95	11	1000	(0.15, 0.20)	Ref. 8
$Ir(cb)_3$/t-DABNA	20.2%	LT50	293	200	(0.13, 0.11)	Ref. 9
PtON7-dtb/v-DABNA	25.4%	LT50	156	1000	(0.14, 0.11)	Ref. 10
PtON-TBBI/TBE2	25.8%	LT95	72.9	1000	(-, 0.165)	Ref. 11

References:

[1] Y. Zhang, S. R. Forrest, *Phys. Rev. Lett.* **2012**, 108, 267404.
[2] S. Reineke, K. Walzer, K. Leo, *Phys. Rev. B* **2007**, 75.
[3] M. Jung, K. H. Lee, J. Y. Lee, T. Kim, *Mater. Horiz.* **2020**, 7, 559.
[4] S. Kim, H. J. Bae, S. Park, W. Kim, J. Kim, J. S. Kim, Y. Jung, S. Sul, S. G. Ihn, C. Noh, S. Kim, Y. You, *Nat. Commun.* **2018**, 9, 1211.
[5] J. Sun, H. Ahn, S. Kang, S.-B. Ko, D. Song, H. A. Um, S. Kim, Y. Lee, P. Jeon, S.-H. Hwang, Y. You, C. Chu, S. Kim, *Nat. Photonics* **2022**, 16, 212.
[6] S. O. Jeon, K. H. Lee, J. S. Kim, S.-G. Ihn, Y. S. Chung, J. W. Kim, H. Lee, S. Kim, H. Choi, J. Y. Lee, *Nat. Photonics* **2021**, 15, 208.
[7] K. H. Choi, K. H. Lee, J. Y. Lee, T. Kim, *Adv. Opt. Mater.* **2019**, 7.
[8] C.-Y. Chan, M. Tanaka, Y.-T. Lee, Y.-W. Wong, H. Nakanotani, T. Hatakeyama, C. Adachi, *Nat. Photonics* **2021**, 15, 203.
[9] K. H. Lee, J. Y. Lee, *J. Mater. Chem. C* **2019**, 7, 8562.
[10] S. Nam, J. W. Kim, H. J. Bae, Y. M. Maruyama, D. Jeong, J. Kim, J. S. Kim, W. J. Son, H. Jeong, J. Lee, S. G. Ihn, H. Choi, *Adv. Sci. (Weinh)* **2021**, 8, e2100586.
[11] E. Kim, J. Park, M. Jun, H. Shin, J. Baek, T. Kim, S. Kim, J. Lee, H. Ahn, J. Sun, S.-B. Ko, S.-H. Hwang, J. Y. Lee, C. Chu, S. Kim, *Sci. Adv.* **2022**, *8*, 41.
[12] S. R. Forrest, *Organic Electronics: Foundations to Applications*, Oxford University Press, **2020**.